THESIS

EVALUATION OF A SURFACE ENERGY BALANCE METHOD BASED ON OPTICAL AND THERMAL SATELLITE IMAGERY TO ESTIMATE ROOT-ZONE SOIL MOISTURE

Submitted by

Nathan E. Alburn

Department of Civil and Environmental Engineering

In partial fulfillments of the requirements

For the Degree of Master of Science

Colorado State University

Fort Collins, Colorado

Fall 2014

Master's Committee:

Advisor: Jeffrey D. Niemann

José L. Chávez
Greg L. Butters

ABSTRACT

EVALUATION OF A SURFACE ENERGY BALANCE METHOD BASED ON OPTICAL AND THERMAL SATELLITE IMAGERY TO ESTIMATE ROOT-ZONE SOIL MOISTURE

Various remote-sensing methods are available to estimate soil moisture, but few address the fine spatial resolutions (e.g., 30 m grid cells) and root-zone depth requirements of agricultural and other similar applications. One approach that has been previously proposed to estimate fine-resolution soil moisture is to first estimate the evaporative fraction from an energy balance that is inferred from optical and thermal remote-sensing images (e.g., using the ReSET algorithm) and then estimate soil moisture through an empirical relationship to evaporative fraction. A similar approach has also been proposed to estimate the degree of saturation. The primary objective of this study is to evaluate these methods for estimating soil moisture and degree of saturation, particularly for a semiarid grassland with relatively dry conditions. Soil moisture was monitored at twenty-eight field locations in southeastern Colorado with herbaceous vegetation during the summer months of three years. In-situ soil moisture and degree of saturation observations are compared with estimates calculated from Landsat imagery using the ReSET algorithm. The in-situ observations suggest that the empirical relationships with evaporative fraction that have been proposed in previous studies typically provide overestimates of soil moisture and degree of saturation in this region. However, calibrated functions produce estimates with an accuracy that may be adequate for various applications. The estimates produced by this approach are more reliable for degree of saturation than for soil moisture, and

the method is more successful at identifying temporal variability than spatial variability in degree of saturation for this region.

ACKNOWLEDGMENTS

We gratefully acknowledge financial support from Colorado State University Agricultural Experiment Station. We thank George McClave, Ron Conrad, Don Higbee, Wendi Rider, and their families for allowing us to utilize their properties for our field research near Lamar. We thank Janet Fleshman, Brian Goss, Jeffrey Linn, Roy Miller, Rich Riddle, Jim Scott, and Mike Stricker for facilitating access to PCMS. We thank Mike Bartolo for the use of the Arkansas Valley Research Center and equipment. We thank John Kuzmiak and Nick Young from USGS for supplying soil moisture and other data. We thank Mike Weber, Jeff Siegfried, Ryan Hemphill, Kevin Werbylo, Devin Traff, Kayla Ranney, and Amber (Brase) Weber for their field assistance. We thank Steve Middlekauff, Mazdak Arabi, Greg Butters, José Chávez, Mike Coleman, Andre Dozier, Darrell Fontane, Tim Gates, Eric Morway, and Lorenz Sutherland for their technical assistance.

TABLE OF CONTENTS

INTRODUCTION

Quantitative knowledge of soil moisture patterns is crucial to making prudent decisions in a wide range of disciplines. Weather forecasting, flood prediction, wildfire mitigation, and mobility assessments can all benefit from soil moisture information (Scott *et al.*, 2003; Hendrickx *et al.*, 2010; Qi *et al.*, 2012; Yebra *et al.*, 2013). Knowledge of soil moisture patterns plays a particularly vital role in agricultural applications. Practices such as precision farming, surge irrigation, and deficit irrigation all hold promise for meeting increasing global needs for food supply, but such practices require detailed and up-to-date knowledge of soil moisture conditions (Moran *et al.*, 1997; Seelan *et al.*, 2003).

Remote-sensing techniques have an advantage over in-situ measurements such as time-domain reflectometry (TDR) because remote-sensing can provide soil moisture estimates over large regions through time. However, passive microwave methods are only sensitive to near-surface soil moisture (the top 5 cm of the soil or less) (Entekhabi *et al.*, 2004; Jackson *et al.*, 2005), and the conditions observed at shallow depths do not necessarily correspond to the conditions throughout the root-zone (Scott *et al.*, 2003; Kerr, 2007), which are more relevant for some applications. Passive microwave estimates also have very coarse spatial resolutions (10 – 40 km grid cells) (Entekhabi *et al.*, 2010), which do not capture fine-scale moisture variations that can also be important (Western *et al.*, 2002; Hendrickx *et al.*, 2011). Airborne active microwave methods, in particular synthetic aperture radar (SAR), have finer spatial resolutions (20 – 100 m) (Moran *et al.*, 2002; Western *et al.*, 2002), but SAR systems have known inaccuracies for smoother and natural surfaces (Altese *et al.*, 1996; Davidson *et al.*, 2000; Walker *et al.*, 2004). In addition, this approach is only sensitive to the soil moisture within about

10 cm of the surface (Ulaby *et al.*, 1996; Walker *et al.*, 2004; Thoma *et al.*, 2008). Because the global average rooting depth is over four meters (Canadell *et al.*, 1996), this approach still misses a large portion of the root-zone soil moisture in much of the world. Even in semiarid regions, grasses can have roots deeper than 10 cm (Weaver, 1958).

An alternative technique to estimate soil moisture with remote sensing is the triangle or trapezoidal method (Moran *et al.*, 1996; Gillies *et al.*, 1997; Carlson, 2007; Stisen *et al.*, 2008). This method utilizes imagery from satellites with visible, infrared, and thermal infrared bands such as Landsat, AVHRR (Advanced Very High Resolution Radiometer), ASTER (Advanced Spaceborne Thermal Emission and Reflection Radiometer), and MODIS (Moderate-resolution Imaging Spectroradimeter). Thus, it can provide estimates with relatively fine spatial resolutions (30 m – 1 km). The trapezoidal method, for example, uses this imagery to make a graph with a vegetation index on one axis and the atmospheric-soil temperature difference on the other (Verstraeten *et al.*, 2008). Four vertices that encompass the data from the region are then identified, which correspond to well-watered vegetation, water-stressed vegetation, saturated bare soil, and dry bare soil. Soil moisture is then estimated by linearly interpolating between the extreme conditions at the vertices of this trapezoid. The trapezoidal method has two key limitations. First, the region must include locations that span the full range of possible vegetation and moisture conditions to properly identify the vertices (Carlson, 2007). Second, the method has an empirical origin, so it may not account properly for topography and other complications or provide reliable quantitative soil moisture estimates in all cases.

Another remote-sensing method to estimate root-zone soil moisture at relatively fine resolutions is based on inferring the components of the land surface energy balance (Bastiaanssen *et al.*, 2000; Scott *et al.*, 2003). This method uses similar spectral bands as the

trapezoidal method and reduces the empiricism associated with the triangle and trapezoidal methods. The first step in this approach is to estimate the net radiation, ground heat, and sensible heat fluxes. The residual of the energy balance is the latent heat flux. These components are then used to calculate either the evapotranspiration (ET) or evaporative fraction (Λ), which is defined as the ratio between the latent heat flux and available energy (net radiation minus soil heat flux) (Shuttleworth *et al.*, 1989; Bezerra *et al.*, 2013). Then, empirical logarithmic functions are used to transform Λ into either root-zone volumetric soil moisture (θ) or degree of saturation (s) (Bastiaanssen *et al.*, 2000; Scott *et al.*, 2003). Several models are available to estimate Λ such as SEBAL (Surface Energy Balance Algorithm for Land) (Bastiaanssen *et al.*, 1998a), SEBS (Surface Energy Balance System) (Su, 1999), S-SEBI (Simplified Surface Energy Balance Index) (Roerink *et al.*, 2000), METRIC (Mapping Evapotranspiration at High Resolution with Internalized Calibration) (Allen *et al.*, 2007), and ReSET (Remote Sensing of Evapotranspiration) (Elhaddad and Garcia, 2008). SEBAL utilizes one weather station with available wind run data. SEBS is similar to SEBAL in its utilization of the energy balance, but it employs more meteorological data in its calculations. S-SEBI also utilizes the energy balance, but approaches the process from a more simplified approach and thus requires only satellite data. METRIC expands upon SEBAL by adding an internal calibration that uses reference ET from weather stations. Finally, ReSET expands upon METRIC by the ability to utilize multiple weather stations for reference ET.

The estimates of ET and Λ from these models have been evaluated in a number of studies (Bastiaanssen *et al.*, 1997; Bastiaanssen *et al.*, 1998b; Morse *et al.*, 2000; Mohamed *et al.*, 2004; Allen *et al.*, 2007; Santos *et al.*, 2010). Santos *et al.* (2010) calculated a mean absolute error (MAE) of 0.30 mm day^{-1} when comparing SEBAL estimated ET and Bowen ratio calculated ET.

SEBAL was also utilized for a water balance study in the upper Nile region with reported errors in ET as high as 27% for one basin and as low as 1.8% and 5.7% for two other basins (Mohamed *et al.*, 2004). Morse *et al*. (2000) also evaluated SEBAL ET estimates and observed greater errors for locations with lower ET values. Using METRIC, Allen *et al*. (2007) reported differences between measured and modeled ET between 4% and 20% and noted that the greatest errors were during drying periods in areas with bare soil. Bastiaanssen *et al.* (1997) compared the Λ estimates from SEBAL to those from flux towers and reported a root mean square error (RMSE) of 0.19. Similarly, in Bastiaanssen *et al*. (1998b), SEBAL Λ estimates were found to have RMSE values between 0.10 and 0.20. Estimates of Λ from S-SEBI were found to have a maximum relative error of 8% (Roerink *et al.*, 2000).

The reliability of θ and *s* estimates from this approach has also been evaluated, but the total number of observations used in these evaluations remains limited. The notion of relating θ and Λ predates these remote-sensing methods and is well established in the literature (Davies and Allen, 1973; Owe and Van De Griend, 1990; Smith *et al.*, 1992). In particular, when the soil is wetter, more of the available energy is expected to be used for ET (latent heat flux), which produces a higher evaporative fraction. However, Bastiaanssen *et al*. (2000) proposed a particular logarithmic relationship between Λ and θ based on data from FIFE (First ISCLCP Field Experiment) (Sellers *et al.*, 1992; Smith *et al.*, 1992) and EFEDA (ECHIVAL Field Experiment in Desertification-Threatened Areas) (Bolle *et al.*, 1993). FIFE was conducted in both grazed and ungrazed grasslands in Kansas. Soil types were primarily alluvium and loess with the soil moisture sensor depth at 2.5 cm. EFEDA was conducted with various vegetation and crop types (vineyards, barley, wheat, maize, and alfalfa) in Spain. Soil types were loamy sand with sensor depths that ranged from 10 cm to 50 cm with 10 cm being the most extensively

evaluated. When fitting the logarithmic function to 23 points from these datasets, Bastiaanssen *et al.* (2000) reported a coefficient of determination (R^2) of 0.855. Scott *et al.* (2003) utilized 27 data points also from both the FIFE and EFEDA sites and estimated a nearly identical relationship. Soils, measurement depths, and vegetation covers were the same for the Bastiaanssen *et al.* (2000) and Scott *et al.* (2003) studies.

Utilizing the data from FIFE and EFEDA, Scott *et al*. (2003) then proposed a modified relationship that replaces θ with *s*, where $s = \theta/\phi$ and ϕ is the soil porosity. This modification was performed to better account for variations in soil type. Scott *et al*. (2003) applied this Λ - *s* relationship to field experiments in the Rechna Doab area in Pakistan and the Lerma-Chapala basin in Mexico. The Rechna Doab sites contain mostly alluvial soils with irrigated rice-wheat and cotton-wheat crop rotations, and observations of *s* were determined by averaging soil moisture values at depth increments of 25 cm in the upper 100 cm of the soil and dividing by the estimated porosities. Porosities were estimated from the highest observed value of θ for each study area. The Lerma-Chapala sites contain vertisols with irrigated wheat, alfalfa, and some strawberries, and soil moisture was measured at 45 cm depth and used to calculate *s*. Ultimately, the RMSE is 0.05 from a comparison of 52 pairs of observed and modeled *s* values. In a related study (Ahmad and Bastiaanssen, 2003), 26 additional points were considered for the same Rechna Doab region, and the parameters of the logarithmic relationship were found to change very little. Fleming *et al.* (2005) evaluated the estimates of *s* produced by this approach for a semiarid region of central New Mexico consisting of mostly grasslands. Soil types were not indicated. The estimates of *s* were compared to in-situ values from 0 – 30 cm depth at eight locations. Good qualitative agreement was found, but quantitative assessments were limited due to the small dataset. Bezerra *et al.* (2013) evaluated the *s* estimates from this approach for

irrigated cotton fields in Brazil. Soils were classified as sandy clay loam. Soil moisture measurements at six depths (10, 20, 30, 40, 60, and 100 cm) were used to determine the root-zone average values of s. Using 24 observations, a RMSE of 0.02 was calculated with Λ ranging from 0.56 to 0.96.

The primary objectives of the present study are to further test the strength of the proposed Λ - θ and Λ - s relationships (Bastiaanssen *et al.*, 2000; Scott *et al.*, 2003) and the reliability of θ and s estimates that are derived from this approach. In particular, the study aims to determine whether the existing relationships that were calibrated using data from particular regions can be reliably applied to other regions. In addition, the study aims to determine whether this methodology is more reliable for estimating θ or s. To calculate the evaporative fraction, Landsat 5 and 7 imagery are used with the ReSET model (Elhaddad and Garcia, 2008), which is similar to SEBAL and METRIC. The model is applied to a semiarid grassland region in southeastern Colorado for the summer months (May through August) of 2009, 2011, and 2012. In-situ soil moisture data were collected and used to estimate θ and s at twenty-eight fields, each of which is meant to correspond to a Landsat grid cell.

The outline of this paper is as follows. The next section "Remote-sensing methods" describes how θ and s were estimated from ReSET. Then, the "Field methods" section describes how the in-situ data were collected. The "Analysis of field data" section evaluates how well the in-situ data represents the average root-zone soil moisture within the Landsat grid cells. Then, the "Results and discussion" section compares the remote-sensing and in-situ estimates, and finally the "Conclusions" section summarizes the main conclusions of the study.

REMOTE-SENSING METHODS

ReSET was utilized in this study for three reasons. First, it expands upon the original SEBAL method by utilizing data from multiple weather stations, which allows the method to better account for spatial variations within the application region. Second, similar to METRIC, ReSET can be calibrated to ground-based reference ET measurements if available. ReSET, however, uses a raster format that allows the usage of multiple weather stations for calibrating the model; such capability is not available in SEBAL or METRIC. Finally, ReSET has been previously applied and tested in the present study's application region and other similar regions (Elhaddad and Garcia, 2008; Elhaddad *et al.*, 2011; Niemann *et al.*, 2011). No innovations or changes were made to ReSET for this study. Thus, only a brief summary of ReSET is provided here, and readers are referred to Elhaddad and Garcia (2008) for a more thorough discussion.

ReSET uses satellite imagery, digital elevation models (DEMs), and surface roughness to calculate the components of the land-surface energy balance equation:

$$\lambda E = R_n - G - H \quad (1)$$

where λE is the latent heat flux (E is the ET rate in $kg \cdot m^{-2} \cdot s^{-1}$ and λ is the latent heat of vaporization of water in $J \cdot kg^{-1}$), R_n is the net radiation at the surface ($W \cdot m^{-2}$), G is soil heat flux ($W \cdot m^{-2}$), and H is the sensible heat flux ($W \cdot m^{-2}$). All terms represent the average values within a given grid cell of the remote-sensing images. Net radiation is computed for each pixel from the radiation balance using surface albedo obtained from short-wave radiation and the emissivity estimated from the long-wave radiation (Bastiaanssen *et al.*, 1998a). Soil heat flux is estimated from net radiation and parameters such as surface albedo, normalized difference vegetation index (NDVI), and surface temperature (Bastiaanssen, 2000). Sensible heat flux is calculated from

wind speed, estimated surface roughness for momentum transport, and air temperature differences between two heights using an iterative process based on the Monin-Obukhov similarity (Monin and Obukhov, 1954). An average Λ for each pixel in the application region is then derived from the components of the energy balance equation:

$$\Lambda \equiv \frac{\lambda E}{\lambda E + H} = \frac{\lambda E}{R_n - G} \quad (2)$$

Satellite data requirements for ReSET include reflectance data in the visible, near-infrared, and infrared bands, as well as emission in the thermal infrared band. For this study, a fine spatial resolution was preferred to facilitate comparison to in-situ measurements, so Landsat 5 and Landsat 7 were used (This study occurred prior to Landsat 8 images being available). Landsat 5 and 7 visible bands (1, 2, and 3) and infrared bands (4, 5, and 7) are all available at a 30 m resolution. Landsat 5 and 7 thermal bands (6) are available at 120 m and 60 m resolutions, respectively. From these data, ReSET produces a Λ grid at a 30 m resolution, but Λ estimates in adjacent 30 m grid cells are not necessarily independent due to the coarser resolution of the thermal bands.

ReSET also requires a DEM and weather station data. A DEM with the same or finer resolution as the satellite data is needed to account for topographic variations in the energy balance components. Wind run values (24-hour) are required from weather stations to estimate the sensible heat flux. ReSET requires the user to determine the extremes on each end of the ET scale: a wet pixel (maximum ET) and a dry pixel (minimum ET). In ReSET's calibrated mode, instantaneous ET is utilized from weather stations to determine the maximum ET value in the processed area and rescale the estimated values. Reference ET values for ReSET's calibrated mode are calculated utilizing the American Society of Civil Engineers (ASCE) Standardized Reference Equation (ASCE-EWRI, 2005) with alfalfa as a reference crop. The required

(weather station) data for this method are air temperature, relative humidity, vapor pressure, solar radiation, and wind speed.

Once the Λ grid is determined, θ and *s* can be calculated from the relationships proposed by Bastiaanssen *et al.* (2000) and Scott *et al*. (2003), respectively. The Bastiaanssen *et al*. (2000) relationship is:

$$\Lambda = a + b\ln(\theta) \text{ or } \theta = e^{\left(\frac{\Lambda - a}{b}\right)} \quad (3)$$

where *a* and *b* are empirical parameters. When fitted through FIFE and EFEDA data, Bastiaanssen *et al*. (2000) and Scott *et al*. (2003) estimated nearly identical values with *a* = 1.284 and *b* = 0.421. The Scott *et al*. (2003) relationship for estimating *s* is:

$$\frac{\theta}{\theta_{sat}} = e^{\left(\frac{\Lambda - c}{d}\right)} \quad (4)$$

where *c* = 1 and *d* = 0.421. Scott *et al*. (2003) imposed *c* = 1 under the expectation Λ = 1 when the soil is fully saturated (*s* = 1). Note that both empirical expressions apply for normal (non-advective) conditions when Λ is expected to range between 0 and 1 (Scott *et al.*, 2003). Thus, the expressions are not expected to hold for low sun angles, cloudy conditions, or areas where well-irrigated crops are surrounded by dry hot areas.

Both θ and *s* were estimated using this approach during summers of 2009, 2011, and 2012 by processing Landsat images 31/34 and 32/34 in southeastern Colorado (Figure 1(a)) when a satellite was over the region and field data were available. The required meteorological data were obtained from four weather stations in the Colorado Agricultural Meteorological Network (CoAgMet) (Andales *et al.*, 2009). Three of these stations are located near Lamar, and the other is near La Junta (Figures 1(a) and (c)). One additional weather station that is operated by Colorado State University (CSU) at the Piñon Canyon Maneuver Site (PCMS) was also used (Melliger and Niemann, 2010). This weather station is co-located with soil moisture probes at

the so-called ungullied site (UNGU), which is described in more detail later. Once θ and *s* maps are developed from ReSET, the θ and *s* values for any instrumented field are determined from a weighted average of any satellite grid cells that overlap the field's spatial extent.

Some estimates of θ and *s* from the remote-sensing method were eliminated from consideration in this study. Landsat 7 images have bands of missing data due to a Scan Line Corrector failure (Barsi *et al.*, 2006), which results in the loss of soil moisture estimates at some fields for some dates. Additional dates and fields were eliminated due to clouds. Several studies have noted that clouds and cloud shadows can create a discrepancy between estimated and actual Λ due to the satellite-perceived temperature differences (Crago and Brutsaert, 1996; Lhomme and Elguero, 1999; Gentine *et al.*, 2007). To avoid any possible effects from clouds, the thermal images were also inspected for any abrupt differences in temperature (typically greater than 5 K over distances less than 500 m) that could not be explained by changes in terrain, irrigation activities, or other physical features. Any sites where the θ and *s* estimates were potentially impacted by clouds were eliminated from analysis. Also, several wildfires burned approximately 18,000 ha in the application region June 5 – 21, 2011 (Michalak and Kriegbaum, 2013). The estimates from three fields during 2011 were excluded from consideration due to close proximity to the burned areas (within 500 m). In addition, 13 sites that were downwind from the burned areas were excluded for June 26, 2011 due to the possibility of smoke over these sites.

FIELD METHODS

The in-situ θ and *s* observations come from three distinct datasets. Two of these datasets are comprised of preexisting sites located at PCMS. PCMS is a large and almost completely undeveloped Army training site that is intermittently used for exercises. The first dataset (CSU PCMS) consists of three fields and was installed for a previous soil moisture study that began in 2008 (Melliger and Niemann, 2010). The second dataset (USGS PCMS) is from the United States Geological Survey (USGS), who installed thirteen sites for prior USGS research projects (Von Guerard *et al.*, 1987; Stevens *et al.*, 2008). Figure 1(a) shows the locations of the CSU PCMS and USGS PCMS fields relative to the Landsat image footprints, and Figure 1(b) shows a closer aerial view of these locations at PCMS. The third dataset (CSU LARV) is comprised of fields that were newly instrumented for this study. These fields are located in the Lower Arkansas River Valley (LARV), which is northeast of PCMS (Figure 1(a)). Twelve fields (six pairs of fields) are included in this dataset (Figure 1(c)).

Vegetation cover at all monitored fields is similar. All fields fall within the same Environmental Protection Agency (EPA) Ecoregion classification, which is: Level 1: Great Plains, Level 2: South Central Semi-Arid Prairies, Level 3: Southwestern Tablelands, Level 4: Piedmont Plains and Tablelands (Omernik, 1987). In addition, all fields are classified by the 2006 National Land Cover Data (NLCD 2006) as grassland/herbaceous. The vegetation consists mainly of shallow root-zone prairie grasses (primarily galleta (Pleuraphis jamesii), alkali sacaton (Sporobolus airoides), sand dropseed (Sporobolus cryptandrus), sideoats grama (Bouteloua curtipendula)) with active root layers typically in the top 50 cm of the soil (Weaver, 1958; Coupland and Johnson, 1965; West *et al.*, 1972). Other species that comprise a small percentage

of the vegetation cover include soapweed yucca (Yucca glauca)), cacti (pinkflower hedgehog (Echinocereus fendleri), kingcup hedgehog (Echinocereus triglochidiatus), and plains prickly pear (Opuntia polyacantha)), Colorado pinyon (Pinus edulis), and juniper (oneseed juniper (Juniperus monosperma) and Rocky Mountain juniper (Juniperus scopulorum)). Some of these species have deeper roots than the herbaceous vegetation and might affect the definition of the root-zone θ and s. For example, yuccas have the potential for rooting depths greater than 6 m (McGinnies *et al.*, 1991). These species were avoided to the extent possible. The depth that is most closely associated with the remote-sensing estimates is examined in more detail later.

CSU PCMS

The CSU PCMS dataset includes three fields, and each field has an extent of approximately one 30 x 30 m Landsat pixel. The westernmost field is identified as ungullied (UNGU), and it has less than 1 m of total relief. The two other fields are located approximately 700 m southeast of UNGU and are referred to as the southwest gully (SWGU) and northeast gully (NEGU). These fields each have a total relief greater than 3 m. NEGU also has a few juniper trees near its eastern edge (within 3 m) but outside the instrumented area. The thermal pixel used to calculate Λ might be impacted by these woody plants and their deeper roots.

Soil moisture at 0-10 cm depth is measured hourly for the CSU PCMS fields using multiple TDR probes that are oriented perpendicular to the soil surface. At UNGU, 32 probes are installed in 4 parallel transects that are 5.5 m apart. Each transect contains 8 probes, which are approximately 6 m apart. Additionally, two locations at UNGU have 10 cm probes buried perpendicular to the soil surface to measure moisture at 10 – 20 cm and 20 – 30 cm depths. SWGU also has 32 surface probes installed in 4 transects, which are 5.5 m apart. Each transect has 8 probes, which are located at the midpoints between breaks in topographic slope. The

average length of each transect at SWGU is approximately 40 m. Additional probes are buried at 2 locations within SWGU to measure soil moisture at 10 – 20 cm and 20 – 30 cm depths. NEGU has 20 surface probes installed in 4 transects, which are 5.5 m apart. Each transect has five probes, which are located at the midpoints between breaks in topographic slope. The average length of each transect at NEGU is approximately 20 m. Additional probes are buried at one location within NEGU to measure soil moisture at 10 – 20 cm and 20 – 30 cm depths.

Campbell Scientific, Inc. (CSI) TDR100's are used to generate the waveforms, and CSI's waveform interpretation algorithm is used to obtain the apparent permittivity (K_a). The Topp *et al*. (Topp *et al.*, 1980) equation is then used to transform K_a to θ. The soil moisture measurements were previously verified by comparing to gravimetrically-derived θ values. The MAE was reported as 0.014 m^3/m^3 by Melliger and Niemann (2010). To remove occasional anomalous soil moisture readings, any individual values greater than two standard deviations from the spatial average for the associated field were eliminated. The remaining values from each field were then used to obtain the final average soil moisture for the field when the satellite was overhead.

The average degree of saturation *s* was then calculated by dividing the average soil moisture by a single average porosity (ϕ) for the field. For each CSU PCMS field, the average porosity was estimated from multiple bulk density values that were measured by Melliger and Niemann (2010) (Table 1). Those authors also collected soil texture information, which suggests that the soils at the CSU PCMS fields are mostly clay loam.

USGS PCMS

Hourly soil moisture is measured at each USGS PCMS field by a single sensor. An Automata Aqua-Tel TDR 94-29 is installed at eight fields, and an Aqua-Tel TDR 630-8019 is

installed at the remaining five fields. All probe lengths are 48.3 cm. The probes are all buried horizontally, but the burial depths range from 3.8 cm to 10.2 cm (Table 1). Soil moisture is derived by an internal waveform interpretation algorithm. Site-specific calibrations were performed by USGS to best reproduce gravimetrically-derived soil moisture observations (Kuzmiak, 2013). Bulk densities were also measured by USGS and have been used to calculate the porosity at each site (Table 1). Soil texture data are not available for these sites, but the USDA NRCS Web Soil Survey indicates that the soil texture is primarily silt loam (Table 1). Vegetation at the USGS PCMS sites is primarily herbaceous, but a few fields (BIGA, CANT, and UBEN) have pinyon pines and junipers that can fall within the thermal pixel used to calculate evaporative fraction. To determine if this vegetation impacts the study results, the three fields in question were temporarily removed from the dataset, and the results did not significantly change.

CSU LARV

Twelve additional fields were instrumented in the LARV to complement the two preexisting datasets. The primary criterion in field selection was to match the vegetation of the preexisting fields. The new fields were selected in the LARV because this region lies in the overlap between the 32/34 and 31/34 image footprints. As a result, remote-sensing estimates can be obtained for these fields approximately every eight days instead of every sixteen days like the PCMS sites. The fields were also selected to avoid areas with high salinity which can impact how easily vegetation can extract the needed moisture and in turn affect the $\Lambda - \theta$ relationship. Fields with heavy grazing, which might affect the relationship between Λ and θ or *s*, due to soil compaction and plant degradation, were also avoided. They were also selected to avoid any feature that could affect the remote-sensing algorithm (a tree, water body, road, etc.). The fields

were also selected to have homogeneous topography and vegetation, where homogeneity was judged based on aerial photos and field inspections. This homogeneity facilitates measurement of the spatial-average θ and s with limited point measurements. In addition, Λ maps were utilized so that the fields as a group span the widest possible range of Λ values (to observe as much of the relationship with θ or s as possible).

Six general areas were selected for fields, and two 30 x 30 m fields were instrumented in each area. The two fields are far enough apart so each field falls in a different pixel in the thermal images (see schematic in Figure 2). Within each field, soil moisture was measured at two locations near the center of the field (and 10 m apart). At each location, an installation hole was excavated, and 15 cm TDR probes were installed with their heads located at 25 cm and 50 cm depths. To avoid any unnatural accumulation of water on top of the probes, they were inserted downward at a 45 degree angle. Thus, the probes measure soil moisture at 25 – 36 cm and 50 – 61 cm depths. The probes were not installed directly above/below each other to avoid possible interactions. In addition, TDR measurements were taken at the surface by inserting a 15 cm probe at a 45 degree angle (measuring soil moisture at 0 – 11 cm depth). Surface measurements were taken within 1 m (but not directly above) the buried probes.

Soil moisture data were collected for the CSU LARV sites only during the summers of 2011 and 2012. On each date when Landsat images were available, a portable CSI TDR100 was used to obtain the soil moisture values. For a given date, location, and depth, three measurements were taken and averaged. The field measurements were collected on the same day as the satellite estimate but not at the exact time of the overpass (approximately 10:30 A.M. MST) because the TDR was transported to each field and measurements were taken manually. The difference in the time of the satellite and in-situ measurements was evaluated as a potential

source of error, but it does not significantly affect the results of the study. CSI's algorithm was used to interpret TDR waveforms and obtain K_a. Then, the K_a values were transformed into soil moisture values using a calibration equation that was developed for each pair of fields using the procedures recommended by Evett *et al.* (2008). The average R^2 value for these equations is 0.98, and the average MAE is 0.007 m^3/m^3 and the average RMSE is 0.008 m^3/m^3 when comparing the TDR soil moisture estimates with gravimetrically-derived soil moisture. To help interpret the intermittent soil moisture measurements from the CSU LARV sites, a Davis Instruments 7852 tipping bucket rain gauge was installed at each field. The rain gauges recorded precipitation values in 0.254 mm increments, which were totaled to obtain hourly rainfall rates.

To calculate *s* at the CSU LARV fields, two soil samples were taken from the top 10 cm in each field. Bulk density values were calculated and used to estimate the porosity. The estimated porosities were compared to the ranges given for the corresponding soil types in the NRCS Web Soil Survey, and all porosity values fell with +/-5% of the ranges.

ANALYSIS OF FIELD DATA

A significant challenge in evaluating remote-sensing estimates is ensuring that the ground measurements are representative of the variable being estimated remotely. For the present study, ensuring comparability between these two sources requires addressing two main issues. First, the remote-sensing method is expected to estimate the spatial-average soil moisture over a 30 m x 30 m grid cell whereas the ground measurements estimate nearly point values at a limited number of locations. Second, the remote-sensing method is expected to estimate the root-zone average soil moisture (Scott *et al.*, 2003; Bezerra *et al.*, 2013) whereas the ground measurements observe particular depths.

First, we examine how well the average soil moisture that is calculated from the two central points at the CSU LARV fields estimates the average soil moisture for a 30 m x 30 m area. For one date at each field, a 5 by 5 grid was surveyed with 6.25 m spacing between each grid point. Surface soil moisture measurements (0 – 11 cm depth) were collected at each of the 25 points using the same procedures that were used for routine monitoring at these fields. The average soil moisture from the 25 temporary points was compared to the average soil moisture from the 2 permanent points. In addition, the quartiles from the 25 points were calculated (Figure 3(a)). For comparison, the quartiles were also calculated for the CSU PCMS fields using the numerous probes that are permanently installed at those fields (Figure 3(b)).

Comparing the box-and-whisker plots in Figure 3 suggests that the CSU LARV fields have much more homogeneous soil moisture than the CSU PCMS fields. This result is expected because the CSU LARV fields were selected to have flat topography and homogeneous vegetation. The average of the two points can fall outside the upper or lower quartiles from the

25 points. However, because the quartiles span such a narrow range at the CSU LARV fields, the actual difference between the two averages is small. On average, the MAE of the 2-point average value is 0.007 m^3/m^3. Considerable spatial variability occurs at the CSU PCMS fields, especially at higher moisture contents (Figure 3(b)). This behavior is also expected given the variable topography in these fields. However, because 20 to 32 locations are monitored on all dates, the estimated average soil moisture is expected to be reliable for the CSU PCMS sites as well.

Spatial variability of soil moisture within the USGS PCMS fields could not be determined due to access restrictions at PCMS. These fields have little topographic relief and generally homogeneous vegetation, so they are expected to resemble the CSU LARV fields more than the CSU PCMS fields. However, only one probe is available at each USGS PCMS field, so these in-situ soil moisture values are expected to be less reliable estimates of the 30 m x 30 m average than the other datasets.

A second analysis was performed to determine whether the surface soil moisture measurements are representative of the depth of soil moisture that is estimated from the remote-sensing method. For this analysis, we considered the fields where soil moisture measurements are available at multiple depths (i.e. CSU LARV and CSU PCMS). For each field, the root-zone average soil moisture was estimated from a weighted average of the in-situ measurements from the three available depths. The weights and the parameters (*a* and *b*) were all simultaneously adjusted to maximize the agreement between the estimated root-zone soil moisture and the remote-sensing estimates based on the Nash Sutcliffe Coefficient of Efficiency (NSCE) (Nash and Sutcliffe, 1970). NSCE has a maximum possible value of one, which would indicate perfect agreement. Lower values indicate worse performance (negative values are possible). The best

agreements occur when the weights of the surface measurements are near 100%. To illustrate this result, Figure 4 includes only the two depths that are consistent in both datasets (surface and 25 cm) and shows the NSCE as the weights are varied. Similar to using three depths, the NSCE is highest when the surface weight approaches 100%. This result suggests that the use of the larger dataset of surface soil moisture measurements to evaluate the remote-sensing estimates is appropriate.

RESULTS AND DISCUSSION

Calibration of the ReSET model to reference ET values from weather stations should improve the accuracy of the Λ estimates, but if weather station data are inaccurate, the calibration could actually introduce errors. Both the uncalibrated and calibrated modes of ReSET were used to process images from the summer of 2009. Figure 5 plots the Λ values from both modes against the in-situ θ measurements from the same subset of dates. For the uncalibrated mode (Figure 5(a)), the Λ values span a very broad range even when θ is small (below 0.2). When the calibrated mode is used, these unexpectedly large Λ values are reduced and the data are more consistent with the proposed Bastiaanssen *et al.* (2000) relationship. In the calibrated mode, the weather station data are used to determine a more reliable upper limit for the ET, which provides an improved estimate for the range. Thus, the calibrated mode produces more realistic results and is used in the remainder of this study.

The complete dataset from all fields and all three summers (280 points) is shown in Figure 6. In particular, Figure 6(a) plots the Λ values from the calibrated mode of ReSET against the in-situ measurements of θ. A large majority of the points (84%) fall above the Bastiaanssen *et al.*(2000) relationship, which implies that for a given θ, Λ is typically higher than expected from that relationship. This disagreement might occur for several reasons. First, it is possible that despite the calibration, ReSET overestimates Λ when θ is small, which shifts the data upwards on the graph. It is also possible that the small dataset used by Bastiaanssen *et al.* (2000) (only 23 points) is not representative of the relationship between Λ and θ for the present application region. For example, the $\Lambda - \theta$ relationship could depend on the sparse vegetation cover and shallow root-zone depth in the region. Leaf area index (LAI) was calculated using the

formula presented in Allen *et al.* (2007), and the average value for all fields was about 0.10. This low value suggests that soil evaporation is likely more important for the present study. Bastiaanssen *et al.* (2000) also used soil moisture measurements as deep as 50 cm, whereas the observations in Figure 6 are all from 0 cm to 11 cm. A shallower root-zone might make any moisture more available for soil evaporation and increase Λ for a given θ. To evaluate the possibility that the depth might play a role, the Bastiaanssen *et al.* (2000) relationship was reevaluated using the deeper soil moisture values that are available in our application region. Some deeper soil moisture values are more consistent with the Bastiaanssen *et al.* (2000) relationship for limited locations and times, but others remain similar to the behavior of the shallow soil moisture data; overall utilizing deeper depths produces greater scatter and poorer performance.

It is also possible that differences in soil texture between the application regions affect the $\Lambda - \theta$ relationship. Previous studies considered sandy clay loam or loamy sand, which have median sand contents of 77% - 83% (Bastiaanssen *et al*., 2000; Scott *et al*., 2003; Bezerra *et al.*, 2013). The majority of the USGS PCMS fields are silt loam, which has a median sand content of 30%. The majority of the CSU LARV fields are loam, which has a median sand content of 50%. Most of the remaining fields are clay loam, which has a median sand content of 50%.

Figure 6(b) plots the Λ values from ReSET against the in-situ measurements of *s*. To generate this figure, the in-situ θ values were converted to *s* by dividing by the porosity estimated for each field. Similar to Figure 6(a), a large majority of the data are above the relationship suggested by Scott *et al.* (2003). Thus, a difference in the typical porosities between the application regions are unlikely to explain the disagreement between the dataset and the relationship proposed by Bastiaanssen *et al.* (2000) that was seen earlier. However, accounting

for the porosity does improve the agreement between the three sources of data for the application region. In Figure 6(a), one can see that the CSU LARV dataset almost always has lower θ values for a given Λ than the CSU PCMS and USGS PCMS datasets. However, the CSU LARV dataset has *s* values that are somewhat more consistent with the other two datasets. This result suggests that Λ might be more directly related to *s* than to θ, but the continued inconsistency between the datasets might suggest that some roles of soil texture remain unaccounted for.

Scott *et al.* (2003) suggested that porosity could potentially be estimated from the maximum observed in-situ soil moisture value. Thus, $s = \theta/\theta_{max}$ where θ_{max} is the largest soil moisture observed at a location. This approach was also implemented, but it produced poorer results than estimating the porosity from the bulk density measurements. Estimating the porosity with this approach is likely less reliable because of the dry conditions that prevailed during the study period and the limited data available at the CSU LARV fields.

Because the data do not agree with the relationships proposed by Bastiaanssen *et al.* (2000) and Scott *et al.* (2003), calibrated relationships were developed to estimate θ and *s* from Λ. Figure 6(a) shows two calibrated relationships to estimate θ. Both relationships have the same logarithmic form as the one proposed by Bastiaanssen *et al.* (2000), but the parameters *a* and *b* were selected to maximize the NSCE of the θ estimates. One of these relationships is also constrained to pass through the point ($\theta = 0.5$, $\Lambda = 1$), which is consistent with the Bastiaanssen *et al.* (2000) relationship. This constraint was added because the large number of very dry points in the dataset overwhelms the influence of the wetter points and produces a very steep relationship if not constrained. Figure 6(b) shows two similarly calibrated relationships to estimate *s*. Both relationships use the *c* and *d* values that maximize the NSCE of the *s* estimates, but one is constrained to pass through ($s = 1$, $\Lambda = 1$), which is consistent with Scott *et al.* (2003).

Figure 7 plots the θ and *s* values that are estimated from the different relationships against the corresponding observed values, and Table 2 summarizes various measures of performance for the θ and *s* estimates. Figure 7(a) shows that using the Bastiaanssen *et al.* (2000) relationship tends to overestimate θ except perhaps at the higher observed values of θ. Similarly, using the Scott *et al.* (2003) relationship tends to overestimate *s* except at the highest observed values of *s* (Figure 7(c)). Both of these tendencies result in the large positive bias values in Table 2. Figure 7(b) and 7(d) show that the calibrated relationships exhibit little bias except at the highest observed θ and *s* values where those relationships tend to provide underestimates. The bias values in Table 2 confirm that the fitted relationships have much less overall bias than the Bastiaanssen *et al.* (2000) and Scott *et al.* (2003) relationships.

The NSCE is negative when the Bastiaanssen *et al.* (2000) relationship is used to estimate θ (Table 2), which suggests a poor ability to reproduce the variability in the observations. The poor NSCE is expected given the substantial bias. The NSCE is still negative when the Scott *et al.* (2003) relationship is used to estimate *s*, but the value is a little better. This improvement again suggests that Λ is more strongly related to *s* than θ. Because using the space-time average of the *s* observations as an estimate would produce an NSCE value of zero, this performance is still quite poor. When the fitted relationships are used to estimate θ, the NSCE values become positive. The RMSE and MAE values for θ are below 0.05 m^3/m^3, which suggests that the method provides an approximate soil moisture estimate that might be suitable for some applications. When the fitted relationships are used to estimate *s*, the NSCE is even better. The RMSE and MAE values for *s* are below 0.09 m^3/m^3, which is again sufficient to provide approximate estimates for *s*. These values are higher than the ones for θ because *s* has a larger

range of variation than θ. In all cases, the mean relative errors (MREs) are quite large in part because many observed θ and *s* values are small.

When calculating the performance metrics described above, values for all locations and dates were combined together. Thus, the metrics consider the method's ability to reproduce both spatial and temporal variability in the dataset. To test whether the method is successful at reproducing spatial variations in *s* on a given date, NSCE was calculated separately for each date and then averaged. When the Scott *et al*. (2003) relationship is used, the average NSCE is -18.8. When the fitted relationship with no constraint is used, the average NSCE increases to -4.56. When the fitted relationship with the constraint to pass through ($s = 1$, $\Lambda = 1$) is used, the NSCE is -4.81. In all cases, the performance varies widely between dates. For the fitted relationship with the constraint, the best day has an NSCE of 0.571, and the worst day has an NSCE of –32.1 (Figure 8(a)). Thus, the remote-sensing method is poor at reproducing the spatial variations in *s* in this dataset. It should be noted that all the fields in the dataset are semiarid grasslands, so the spatial variations in moisture are relatively small. If, for example, wetter points from irrigated fields were included in the dataset, it is very likely that the method would identify those points as wetter and the spatial variability that is reproduced would increase substantially. Nonetheless, these results suggest that the method is poor at differentiating the moisture values that occur across the naturally-vegetated portions of this relatively flat and homogeneous landscape.

A similar analysis was performed to examine the method's ability to reproduce the temporal variability at each field. The NSCE was calculated separately for each field and then averaged. Using the Scott *et al.* (2003) parameters ($a = 1$, $b = 0.421$), the average NSCE is -2.87, best NSCE at any field is 0.746, and the worst is -15.5. When the fitted relationship without the constraint is used, the average NSCE is 0.141. When the fitted relationship with the constraint is

used, the average NSCE is -0.043. For this last case, the best NSCE at any field is 0.808, and the worst NSCE at any field is -1.72 (Figure 8(b)). Thus, the remote-sensing method is more successful at reproducing temporal variability than spatial variability in this dataset. This result likely occurs because a wider variation in moisture occurs through time in each field in the dataset than occurs between different fields on a given date.

The dataset was partitioned in a variety of other ways to try to identify more specific sources of error. For example, the data were separated into groups based on the time since the most recent rainfall event to investigate whether rainfall disturbs the relationships with Λ. Rainfall can potentially increase the soil moisture quicker than plants can transpire the available water (Laio *et al.*, 2001). In addition, soil heat flux is also quickly impacted by rainfall events (Cammalleri *et al.*, 2012). However, the error does not exhibit a clear dependence on the time following the most recent rainfall event or other factors considered. In addition, the possibility that Λ is related to an average s over a preceding period of time was considered. The soil moisture observations at each location were used to calculate the average s over varying periods (up to 2 weeks) leading up to the time when Λ is estimated from ReSET. However, Λ is most strongly related to s at the coincident time.

The remaining errors might stem from a variety of sources. The Λ values likely include some errors. For example, ReSET assumes that the aerodynamic roughness is homogeneous, and various studies have indicated that variability in the aerodynamic roughness can impact the estimates of the surface fluxes (Hignett, 1994; Prueger *et al.*, 2004; Lu *et al.*, 2009; Chávez *et al.*, 2012). Although the fields in this study were selected to be as homogeneous as possible, vegetation heights do vary and bare patches do occur within the fields. Other errors might stem from the use of a unique relationship between Λ and s. Modeling studies have shown substantial

scatter in the soil moisture values that are associated with a given transpiration rate (Entekhabi *et al.*, 1992; Tripp and Niemann, 2008). Such scatter can occur if plants extract water from one layer to compensate for dry conditions in another layer. It could also occur due to hysteresis in relationship between soil moisture and the suction head, which is likely more closely related to Λ. Such scatter would make it difficult to estimate soil moisture from the transpiration rate by way of a single static equation. The density of vegetation cover has also been shown to impact the relationship between evaporative fraction and soil moisture (Jamiyansharav *et al.*, 2011; Krishnan *et al.*, 2012). ET from bare areas is dominated by soil evaporation, which is expected to extract water from near the surface. On the other hand, ET from more densely vegetated areas has a higher contribution from transpiration and is expected to extract water from deeper in the soil. Thus, the depth that is most closely associated with evaporative fraction is expected to vary in space and potentially in time.

CONCLUSIONS

The main objectives of this study were to test the strength of the proposed Λ - θ and Λ - s relationships and to evaluate the estimation of θ and s when Λ is inferred from optical and thermal imagery. The main conclusions from this study are as follows:

1. For the semiarid grassland where this study was conducted, the estimates of θ and s from the remote-sensing method are most strongly related to soil moisture in the top 10 cm of the soil. The roots of the herbaceous vegetation in this region can reach 50 cm in depth and the roots of other particular species (e.g., yuccas) can reach much deeper. However, the shallow soil moisture likely plays a strong role because a large proportion of the total roots are near the surface and because evaporation from bare patches of soil also contributes significantly to Λ.
2. The empirical relationship between Λ and θ that was proposed by Bastiaanssen *et al.* (2000) and the empirical relationship between Λ and s that was proposed Scott *et al.* (2003) are not universally applicable. In the application region, these equations overestimate θ and s when supplied with Λ from ReSET. This bias also leads to negative NSCE values for the θ and s estimates. However, if calibrated relationships are determined using the in-situ observations, the biases in the estimates of θ and s are substantially smaller and the NSCE values become positive. Furthermore, the RMSE and MAE values suggest that the method can be used to gain rough approximations of θ or s.
3. Estimates produced by the remote-sensing method are somewhat more reliable for s than θ. For a given Λ, the in-situ θ values are consistently lower in the LARV region than the PCMS region while the in-situ s values are a bit more consistent between the regions. In

addition, the NSCE values for the *s* estimates are higher than the NSCE values for the θ estimates. This suggests that Λ is more directly related to *s* than θ. However, some inconsistency persists between the sites with different soils when estimating *s*, which might suggest that some roles of soil texture are not fully resolved by replacing θ with *s*.

4. This method is more successful at capturing temporal variation than spatial variation for this relatively homogeneous grassland. The poor ability to reproduce spatial variations probably occurs because relatively little variation in θ or *s* is observed between different locations on the same date. In contrast, relatively large variations occurred between different dates at the same locations, which are more easily detected.

Overall these results confirm that an association between Λ and *s* occurs. However, the precise form of the relationship differs between the dataset collected here and those from other regions. In addition, considerable scatter occurs around the relationship. Further research is needed to gain a better understanding of the physical origin of this relationship, the site characteristics that can affect the relationship, and the times and locations when the relationship is stronger and weaker. Additional research should also determine whether related methods such as SEBAL, SEBS, S-SEBI, and METRIC can produce improved results.

TABLES AND FIGURES

Table 1. Soil moisture measurement depth, soil type, and average porosity values for each field. Data sources are identified by their region and the organization that collected the data. PCMS is Pinon Canyon Maneuver Site, and LARV is the Lower Arkansas River Valley. USGS is the United States Geological Survey, and CSU is Colorado State University. Each field is then given a unique four character designation. For example, the three CSU PCMS fields are Northeast Gully (NEGU), Southwest Gully (SWGU), and Ungullied (UNGU).

Data Source	Field	Measurement Depth (cm)	USDA Soil Classification	Average Porosity
USGS PCMS	BEAR	7.6	silt loam	0.53
	BIGA	5.1	silt loam	0.52
	BRSH	3.8	loam	0.47
	BURS	7.6	silt loam	0.53
	CANT	10.2	silt loam	0.54
	CAWM	7.6	silt loam	0.55
	CIGS	7.6	clay loam	0.52
	GUTI	10.2	silty clay loam	0.58
	MINC	7.6	clay loam	0.50
	ROUR	7.6	silt loam	0.57
	RTWM	3.8	silt loam	0.57
	UBEN	7.6	clay loam	0.55
	URED	7.6	sandy loam	0.45
CSU PCMS	NEGU	0 - 10	clay loam	0.49
	SWGU	0 - 10	clay loam	0.49
	UNGU	0 - 10	silty clay loam	0.50
CSU LARV	LA1E	0 - 11	loam	0.43
	LA1W	0 - 11	loam	0.46
	LA2E	0 - 11	loam	0.43
	LA2W	0 - 11	loam	0.46
	LA3E	0 - 11	loam	0.46
	LA3W	0 - 11	loam	0.46
	LA4E	0 - 11	loam	0.45
	LA4W	0 - 11	loam	0.48
	LA5E	0 - 11	clay loam	0.43
	LA5W	0 - 11	clay loam	0.46
	LA6E	0 - 11	sandy loam	0.46
	LA6W	0 - 11	sandy loam	0.36

Table 2. Measures of performance when various relationships are used to estimate θ and *s*.

Variable Estimated	Relationship Used	NSCE	RMSE	MAE	MRE	BIAS
θ	Bastiaanssen *et al.* (2000)	-1.116	0.075	0.064	100%	0.058
	Fitted Equation	0.322	0.042	0.032	42%	-0.0004
	Fitted and Forced Through ($\theta = 0.5$, $\Lambda = 1$)	0.260	0.044	0.034	43%	-0.0022
s	Scott *et al.* (2003)	-1.017	0.141	0.117	90%	0.109
	Fitted Equation	0.355	0.079	0.061	39%	-0.0008
	Fitted and Forced Through ($s = 1$, $\Lambda = 1$)	0.288	0.084	0.065	41%	-0.0056

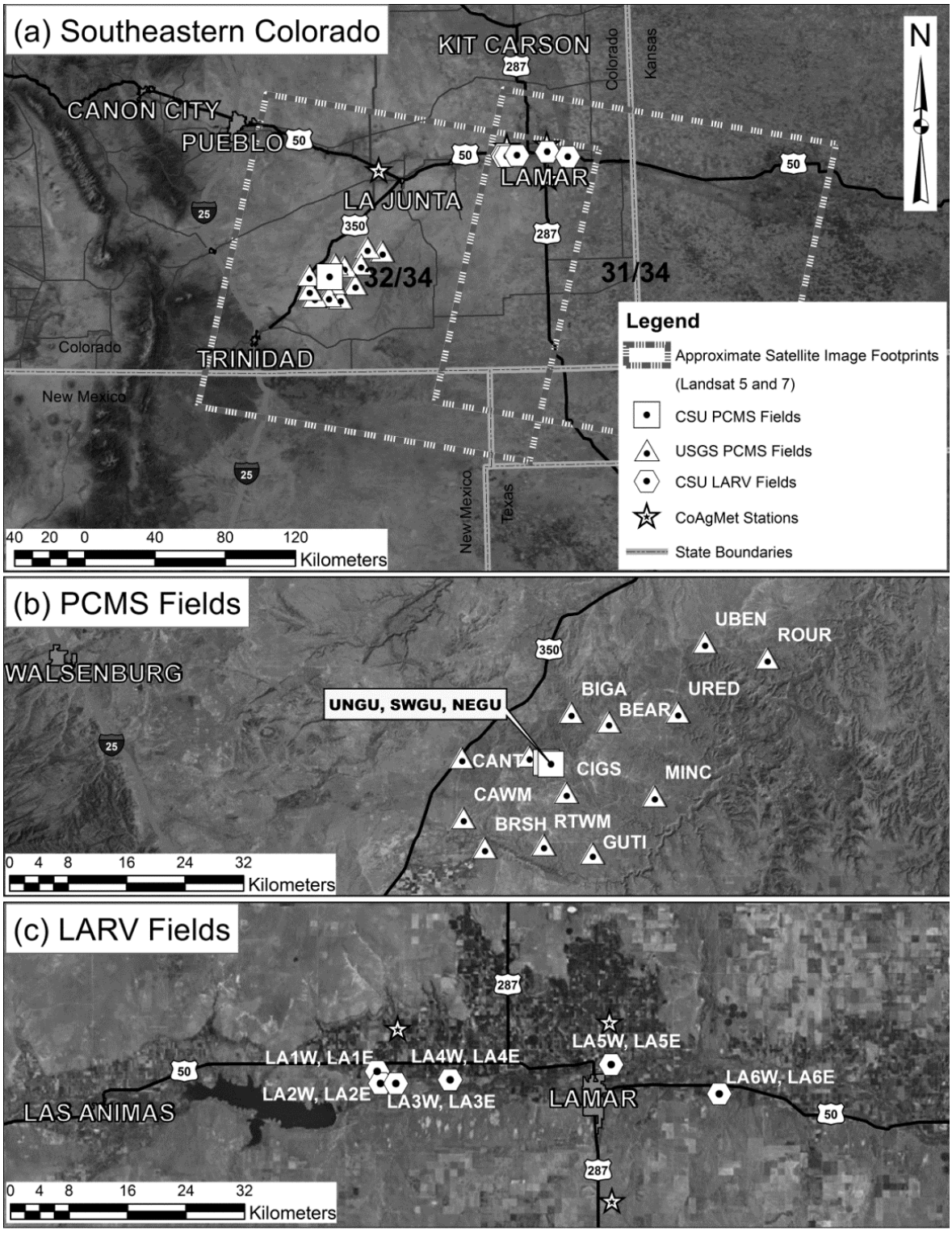

Figure 1. (a) Application region with approximate Landsat 5 and 7 image footprints (32/34, 31/34) and instrumented field locations. (b) A zoomed view of the PCMS region with instrumented fields. (c) A zoomed view of the LARV region with the instrumented fields shown (adjacent east and west fields too close to be distinguished in the figure).

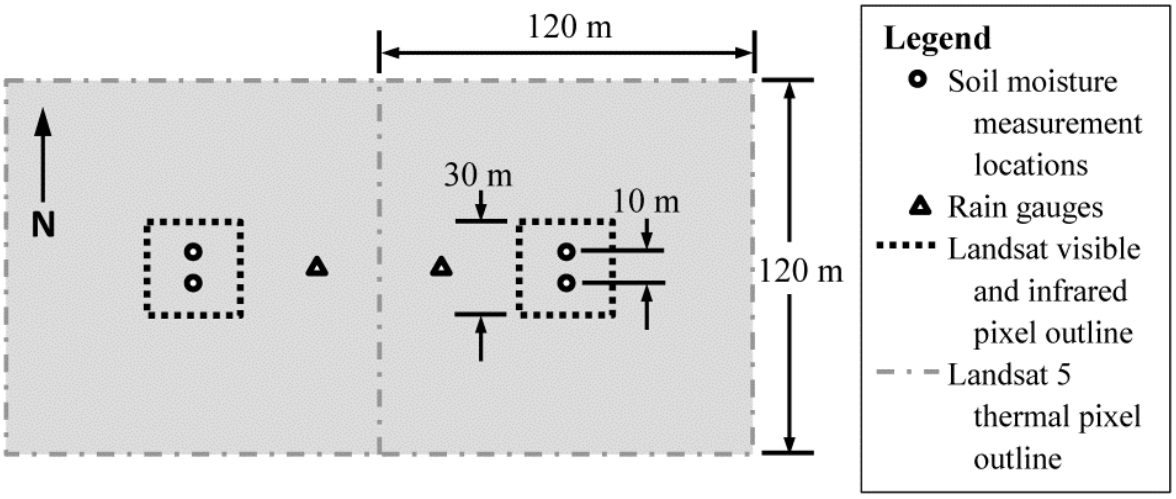

Figure 2. Schematic diagram showing the instrumentation layout for a pair of fields in the CSU LARV dataset.

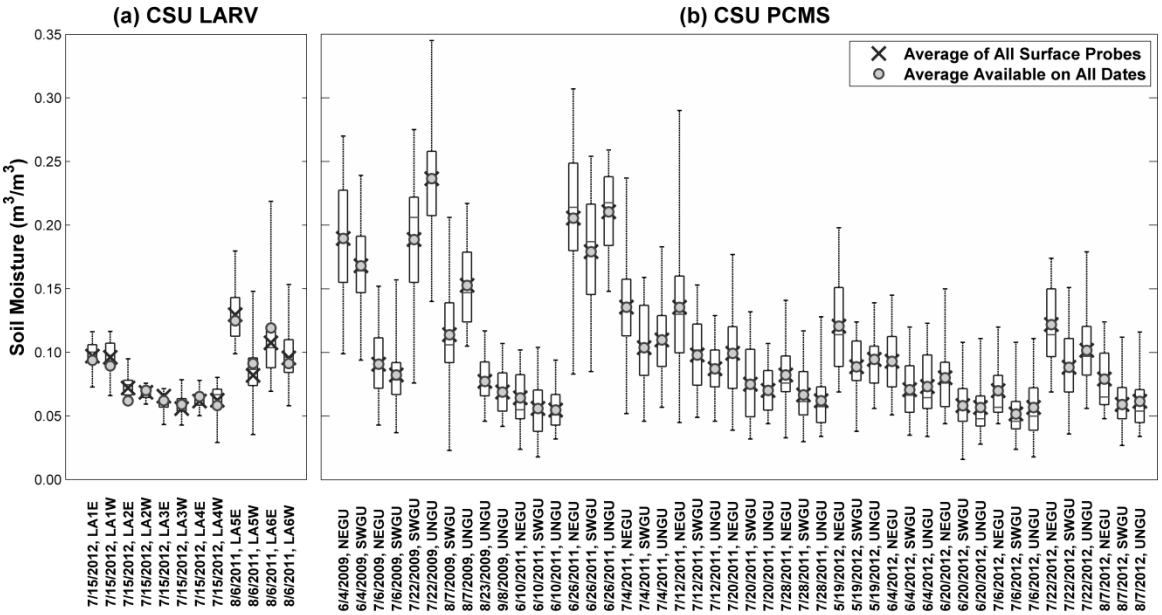

Figure 3. Characterization of the spatial variability of soil moisture within the CSU LARV and CSU PCMS fields for all available dates. Upper and lower edges of the boxes correspond to upper and lower quartiles, and the upper and lower limits of the whiskers indicate maximum and minimum values.

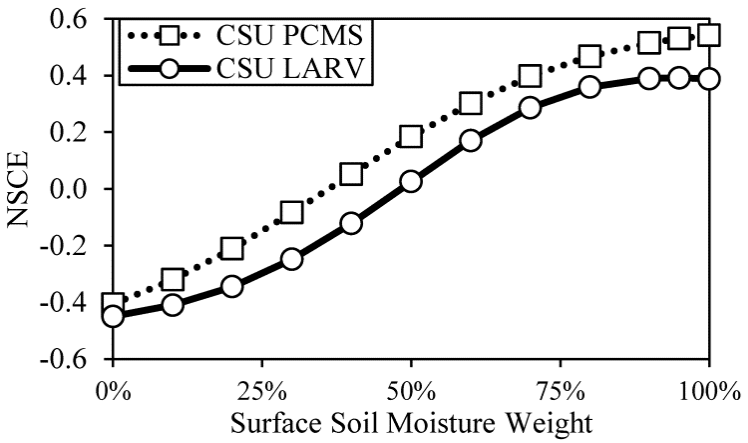

Figure 4. NSCE when estimates of θ from the remote-sensing method are compared with in-situ values that are calculated from a weighted average of measurements at two depths (surface and 25 cm) common to both data sets.

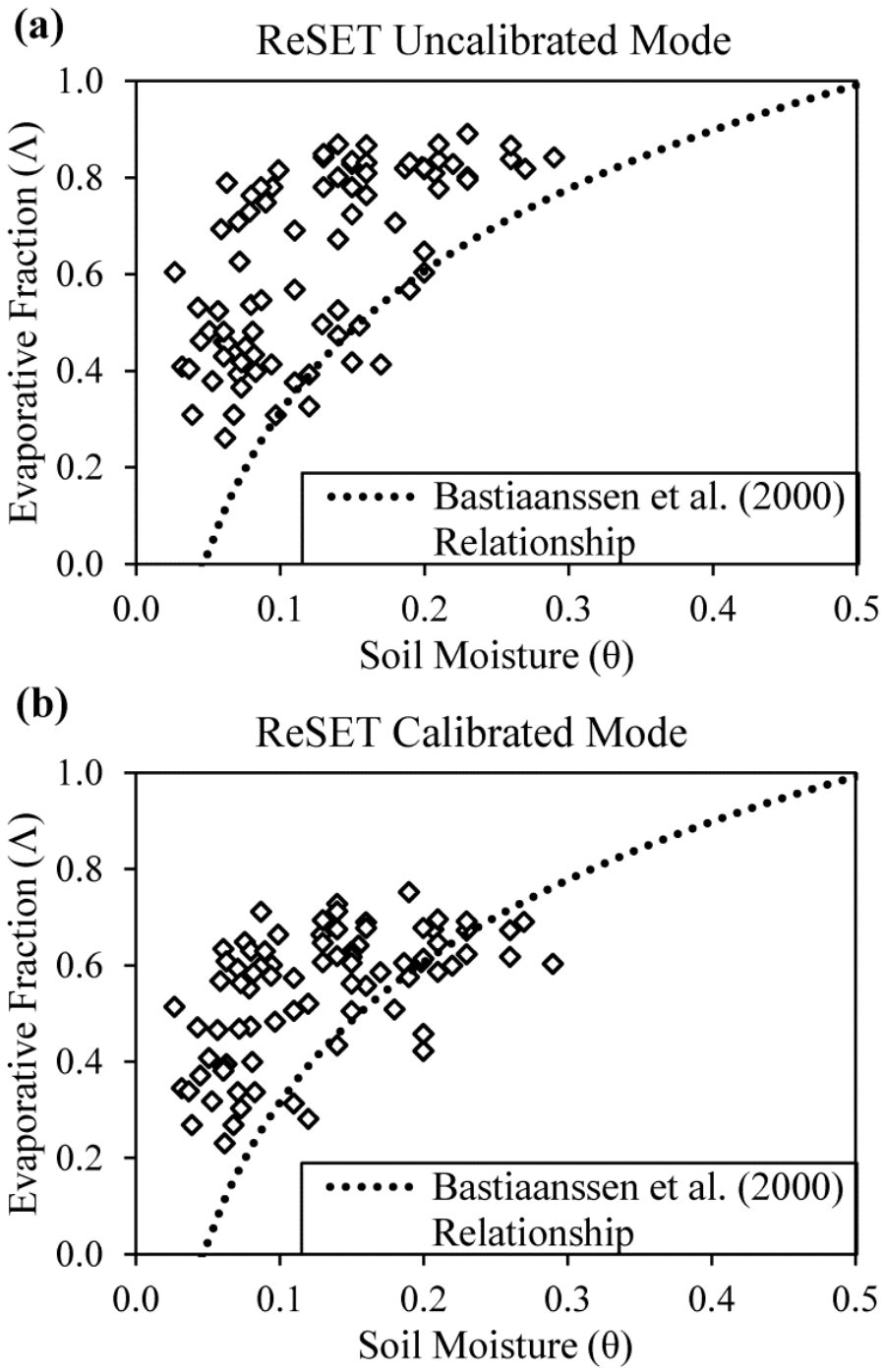

Figure 5. Evaporative fraction calculated using ReSET's (a) uncalibrated mode and (b) calibrated mode. These values are plotted against the surface in-situ soil moisture measurements that are available from 2009 (only CSU PCMS and USGS PCMS data).

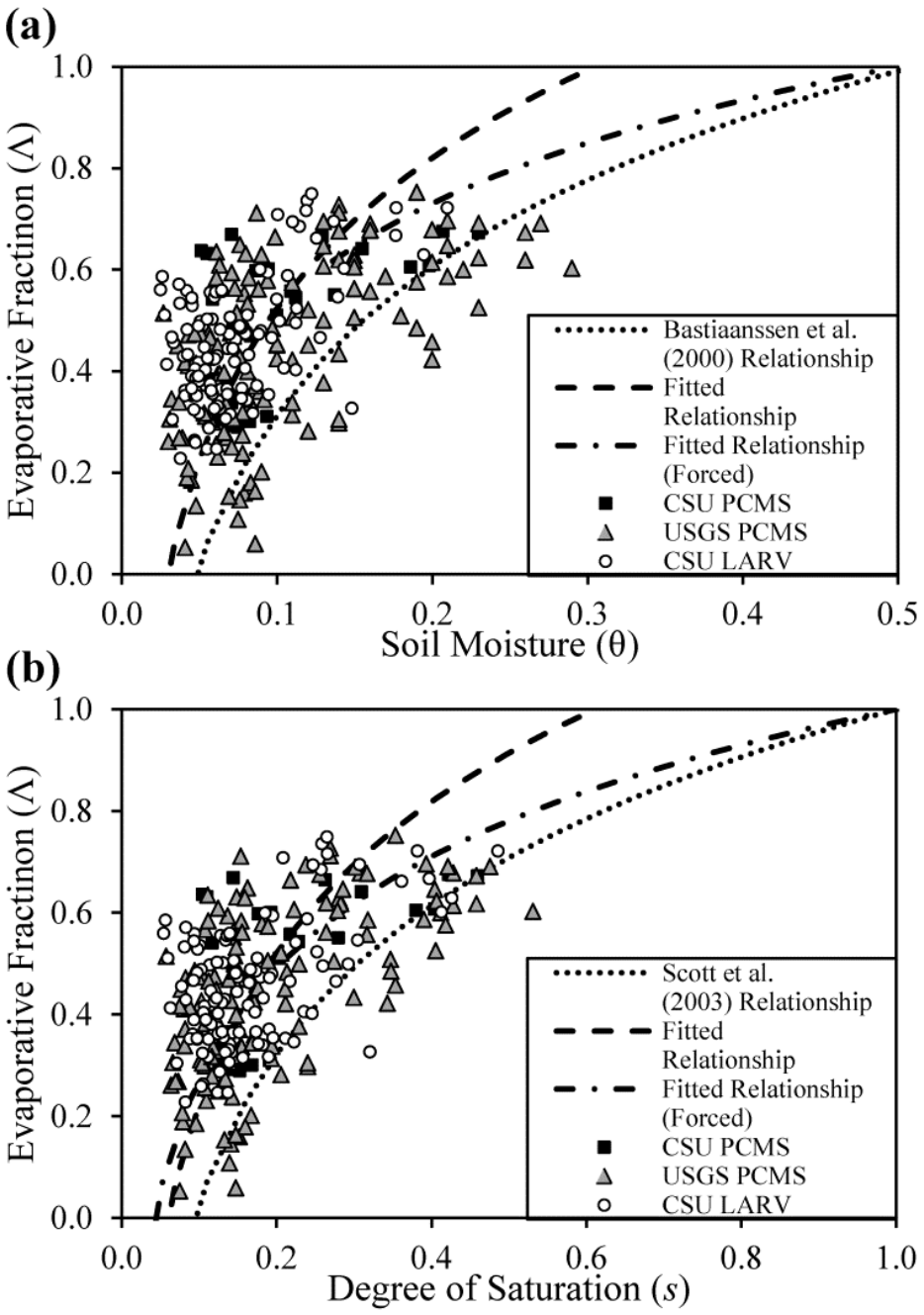

Figure 6. Evaporative fraction plotted against (a) in-situ surface soil moisture measurements and (b) degree of saturation values. Graphs include data from all available dates and locations (280 points). The fitted relationship to estimate θ uses a = 1.508 and b = 0.427. The fitted relationship for θ that includes the constraint uses a = 1.204 and b = 0.294. The fitted relationship to estimate s uses c = 1.211 and d = 0.428. The fitted relationship for s that includes the constraint uses c = 1 and d = 0.294.

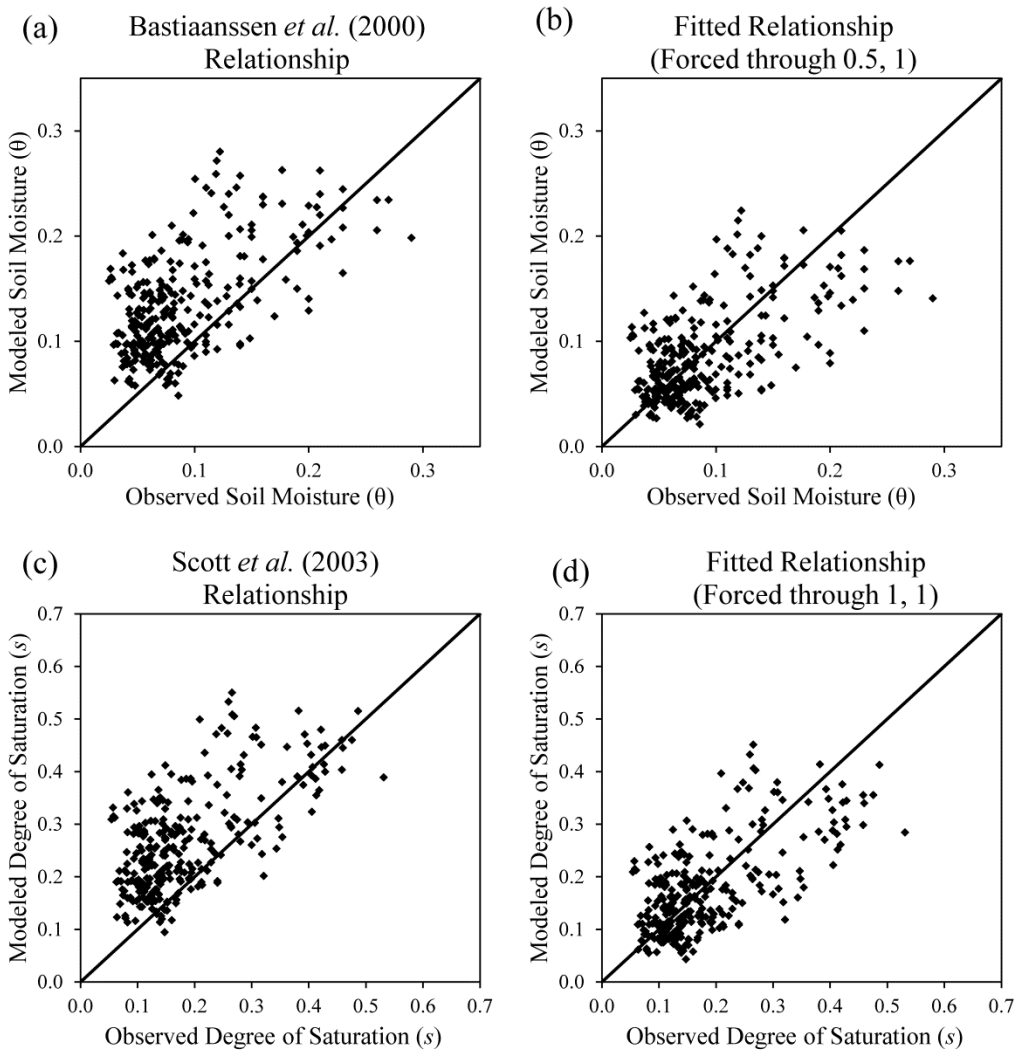

Figure 7. Comparisons of estimated θ or *s* values against observed θ or *s* values as indicated in the plots. (a) Uses the Bastiaanssen *et al.* (2000) relationship, (b) uses the fitted relationship that is forced through ($\theta = 0.5$, $\Lambda = 1$), (c) uses the Scott *et al.* (2003) relationship, and (d) uses the fitted relationship for *s* that is forced through ($s = 1$, $\Lambda = 1$).

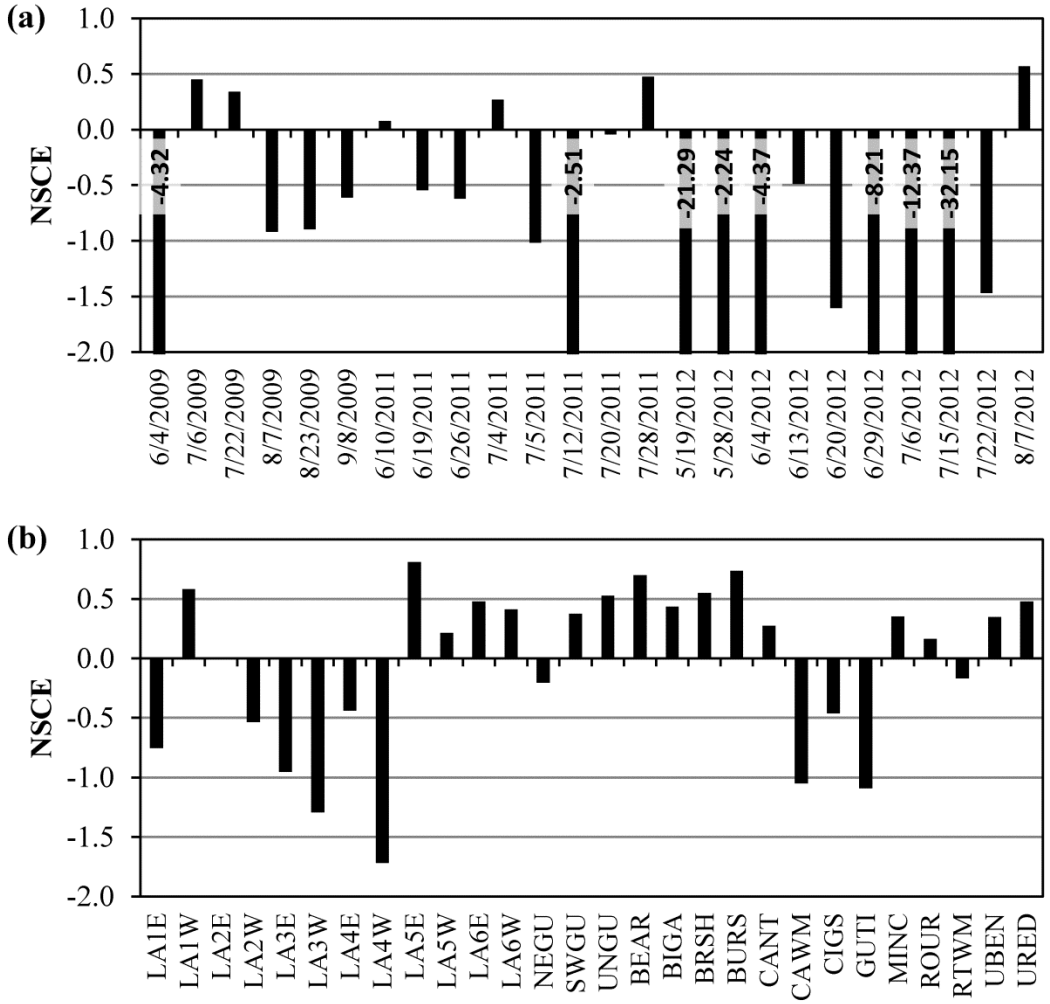

Figure 8. (a) NSCE values calculated separately for each date and (b) NSCE values calculated separately for each location.

REFERENCES

Ahmad M-u-D, Bastiaanssen WGM. 2003. Retrieving Soil Moisture Storage in the Unsaturated Zone Using Satellite Imagery and Bi-Annual Phreatic Surface Fluctuations. Irrigation and drainage systems, **17**: 141-161. DOI: 10.1023/a:1025101217521.

Allen R, Tasumi M, Trezza R. 2007. Satellite-Based Energy Balance for Mapping Evapotranspiration with Internalized Calibration (METRIC)—Model. Journal of irrigation and drainage engineering, **133**: 380-394. DOI: 10.1061/(ASCE)0733-9437(2007)133:4(380).

Altese E, Bolognani O, Mancini M, Troch PA. 1996. Retrieving Soil Moisture Over Bare Soil from ERS 1 Synthetic Aperture Radar Data: Sensitivity Analysis Based on a Theoretical Surface Scattering Model and Field Data. Water Resources Research, **32**: 653-661. DOI: 10.1029/95wr03638.

Andales AA, Bauder TA, Doesken NJ. 2009. The Colorado Agricultural Meteorological Network, CoAgMet, and Crop ET Reports. Colorado State University Extension, pp: 1-3.

ASCE-EWRI. 2005. The ASCE Standardized Reference Evapotranspiration Equation. Environmental and Water Resources Institue (EWRI) of American Society of Civil Engineers (ASCE), Standardization of Reference Evapotranspiration Task Committee Final Report.

Barsi JA, Hook SJ, Palluconi FD, Schott JR, Raqueno NG. 2006. Landsat TM and ETM+ thermal band calibration. In: Optics & Photonics, International Society for Optics and Photonics, pp: 62960F-62960F-62969.

Bastiaanssen WGM. 2000. SEBAL-based sensible and latent heat fluxes in the irrigated Gediz Basin, Turkey. Journal of hydrology, **229**: 87-100. DOI: 10.1016/s0022-1694(99)00202-4.

Bastiaanssen WGM, Menenti M, Holtslag AAM, Feddes RA. 1998a. A remote sensing surface energy balance algorithm for land (SEBAL). 1. Formulation. Journal of hydrology, **212**: 198-212.

Bastiaanssen WGM, Molden DJ, Makin IW. 2000. Remote sensing for irrigated agriculture: examples from research and possible applications. Agricultural Water Management, **46**: 137-155. DOI: 10.1016/S0378-3774(00)00080-9.

Bastiaanssen WGM, Pelgrum H, Droogers P, de Bruin HAR, Menenti M. 1997. Area-average estimates of evaporation, wetness indicators and top soil moisture during two golden days in EFEDA. Agric. For. Meteorol., **87**: 119-137. DOI: 10.1016/s0168-1923(97)00020-8.

Bastiaanssen WGM, Pelgrum H, Wang J, Ma Y, Roerink GJ, Moreno JF. 1998b. A remote sensing surface energy balance algorithm for land (SEBAL). 2. Validation. Journal of hydrology, **212**: 213-229.

Bezerra BG, dos Santos CAC, da Silva BB, Perez-Marin AM, Bezerra MVC, Bezerra JRC, Rao TVR. 2013. Estimation of soil moisture in the root-zone from remote sensing data. Rev. Bras. Cienc. Solo, **37**: 596-603.

Bolle HJ, DeBruin HAR, Stricker H. 1993. EFEDA: European field experiment in a desertification threatened area. Annales geophysicae, **11**: 173-189.

Cammalleri C, Ciraolo G, La Loggia G, Maltese A. 2012. Daily evapotranspiration assessment by means of residual surface energy balance modeling: A critical analysis under a wide

range of water availability. Journal of hydrology, **452–453**: 119-129. DOI: 10.1016/j.jhydrol.2012.05.042.
Canadell J, Jackson RB, Ehleringer JB, Mooney HA, Sala OE, Schulze ED. 1996. Maximum rooting depth of vegetation types at the global scale. Oecologia, **108**: 583-595. DOI: 10.1007/bf00329030.
Carlson T. 2007. An Overview of the "Triangle Method" for Estimating Surface Evapotranspiration and Soil Moisture from Satellite Imagery. Sensors, **7**: 1612-1629.
Chávez J, Gowda P, Howell T, Garcia L, Copeland K, Neale C. 2012. ET Mapping with High-Resolution Airborne Remote Sensing Data in an Advective Semiarid Environment. Journal of irrigation and drainage engineering, **138**: 416-423. DOI: doi:10.1061/(ASCE)IR.1943-4774.0000417.
Coupland RT, Johnson RE. 1965. Rooting Characteristics of Native Grassland Species in Saskatchewan. Journal of Ecology, **53**: 475-507. DOI: 10.2307/2257990.
Crago R, Brutsaert W. 1996. Daytime evaporation and the self-preservation of the evaporative fraction and the Bowen ratio. Journal of hydrology, **178**: 241-255. DOI: 10.1016/0022-1694(95)02803-X.
Davidson M, Thuy Le T, Mattia F, Satalino G, Manninen T, Borgeaud M. 2000. On the characterization of agricultural soil roughness for radar remote sensing studies. Geoscience and Remote Sensing, IEEE Transactions on, **38**: 630-640. DOI: 10.1109/36.841993.
Davies JA, Allen CD. 1973. Equilibrium, Potential and Actual Evaporation from Cropped Surfaces in Southern Ontario. Journal of Applied Meteorology, **12**: 649-657. DOI: 10.1175/1520-0450(1973)012<0649:epaaef>2.0.co;2.
Elhaddad A, Garcia L. 2008. Surface Energy Balance-Based Model for Estimating Evapotranspiration Taking into Account Spatial Variability in Weather. Journal of irrigation and drainage engineering, **134**: 681-689. DOI: 10.1061/(ASCE)0733-9437(2008)134:6(681).
Elhaddad A, Garcia L, Chávez JL. 2011. Using a Surface Energy Balance Model to Calculate Spatially Distributed Actual Evapotranspiration. Journal of irrigation and drainage engineering, **137**: 17-26. DOI: doi:10.1061/(ASCE)IR.1943-4774.0000276.
Entekhabi D, Njoku EG, Houser P, Spencer M, Doiron T, Yunjin K, Smith J, Girard R, Belair S, Crow W, Jackson TJ, Kerr YH, Kimball JS, Koster R, McDonald KC, O'Neill PE, Pultz T, Running SW, Jiancheng S, Wood E, Van Zyl J. 2004. The hydrosphere State (hydros) Satellite mission: an Earth system pathfinder for global mapping of soil moisture and land freeze/thaw. Geoscience and Remote Sensing, IEEE Transactions on, **42**: 2184-2195. DOI: 10.1109/tgrs.2004.834631.
Entekhabi D, Njoku EG, O'Neill PE, Kellogg KH, Crow WT, Edelstein WN, Entin JK, Goodman SD, Jackson TJ, Johnson J, Kimball J, Piepmeier JR, Koster RD, Martin N, McDonald KC, Moghaddam M, Moran S, Reichle R, Shi JC, Spencer MW, Thurman SW, Leung T, Van Zyl J. 2010. The Soil Moisture Active Passive (SMAP) Mission. Proceedings of the IEEE, **98**: 704-716. DOI: 10.1109/jproc.2010.2043918.
Entekhabi D, Rodriguez-Iturbe I, Bras RL. 1992. Variability in Large-Scale Water Balance with Land Surface-Atmosphere Interaction. Journal of Climate, **5**: 798-813. DOI: 10.1175/1520-0442(1992)005<0798:vilswb>2.0.co;2.
Evett SR, Cepuder P, Heng LK, Hignett C, Laurent JP, Ruelle P. 2008. Field estimation of soil water content: A practical guide to methods, instrumentation and sensor technology. In:

Training Course Series 30, Evett SR (ed.) International Atomic Energy Agency, pp: 68-70.
Fleming K, Hendrickx JMH, Hong S-h. 2005. Regional mapping of root zone soil moisture using optical satellite imagery. pp: 159-170.
Gentine P, Entekhabi D, Chehbouni A, Boulet G, Duchemin B. 2007. Analysis of evaporative fraction diurnal behaviour. Agric. For. Meteorol., **143**: 13-29. DOI: 10.1016/j.agrformet.2006.11.002.
Gillies RR, Kustas WP, Humes KS. 1997. A verification of the 'triangle' method for obtaining surface soil water content and energy fluxes from remote measurements of the Normalized Difference Vegetation Index (NDVI) and surface e. International journal of remote sensing, **18**: 3145-3166. DOI: 10.1080/014311697217026.
Hendrickx JMH, Harrison BJ, Borchers B, Rodríguez-Marín G, Howington S, Ballard J. 2010. High-resolution soil moisture mapping using operational optical satellite imagery. pp: 76641O-76641O-76614.
Hendrickx JMH, Harrison JBJ, Borchers B, Kelley JR, Howington S, Ballard J. 2011. High-resolution soil moisture mapping in Afghanistan. In: Detection and Sensing of Mines, Explosive Objects, and Obscured Targets Xvi, Harmon RS, Holloway JH, Broach JT (eds.) Spie-Int Soc Optical Engineering.
Hignett P. 1994. Roughness lengths for temperature and momentum over heterogeneous terrain. Boundary-Layer Meteorology, **68**: 225-236. DOI: 10.1007/bf00705598.
Jackson TJ, Bindlish R, Gasiewski AJ, Stankov B, Klein M, Njoku EG, Bosch D, Coleman TL, Laymon CA, Starks P. 2005. Polarimetric scanning radiometer C- and X-band microwave observations during SMEX03. Geoscience and Remote Sensing, IEEE Transactions on, **43**: 2418-2430. DOI: 10.1109/tgrs.2005.857625.
Jamiyansharav K, Ojima D, Pielke RA, Parton W, Morgan J, Beltrán-Przekurat A, LeCain D, Smith D. 2011. Seasonal and interannual variability in surface energy partitioning and vegetation cover with grazing at shortgrass steppe. Journal of Arid Environments, **75**: 360-370. DOI: 10.1016/j.jaridenv.2010.11.008.
Kerr YH. 2007. Soil moisture from space: Where are we? Hydrogeology journal, **15**: 117-120.
Krishnan P, Meyers TP, Scott RL, Kennedy L, Heuer M. 2012. Energy exchange and evapotranspiration over two temperate semi-arid grasslands in North America. Agric. For. Meteorol., **153**: 31-44. DOI: 10.1016/j.agrformet.2011.09.017.
Kuzmiak J. 2013. Citation and calibration question. Alburn N (ed.).
Laio F, Porporato A, Ridolfi L, Rodriguez-Iturbe I. 2001. Plants in water-controlled ecosystems: active role in hydrologic processes and response to water stress: II. Probabilistic soil moisture dynamics. Advances in Water Resources, **24**: 707-723. DOI: 10.1016/S0309-1708(01)00005-7.
Lhomme JP, Elguero E. 1999. Examination of evaporative fraction diurnal behaviour using a soil-vegetation model coupled with a mixed-layer model. Hydrol. Earth Syst. Sci., **3**: 259-270. DOI: 10.5194/hess-3-259-1999.
Lu L, Liu S, Xu Z, Yang K, Cai X, Jia L, Wang J. 2009. The characteristics and parameterization of aerodynamic roughness length over heterogeneous surfaces. Adv. Atmos. Sci., **26**: 180-190. DOI: 10.1007/s00376-009-0180-3.
McGinnies WJ, Shantz HL, McGinnies WG. 1991. Changes in vegetation and land use in eastern Colorado: A photographic study, 1904-1986. ARS-US Department of Agriculture, Agricultural Research Service (USA).

Melliger JJ, Niemann JD. 2010. Effects of gullies on space–time patterns of soil moisture in a semiarid grassland. Journal of hydrology, **389**: 289-300. DOI: 10.1016/j.jhydrol.2010.06.006.

Michalak K, Kriegbaum R. 2013. Wildfire in Colorado: Preliminary Report on the 2012 Wildfire Season. Colorado Division of Fire Prevention and Control, pp: 27.

Mohamed YA, Bastiaanssen WGM, Savenije HHG. 2004. Spatial variability of evaporation and moisture storage in the swamps of the upper Nile studied by remote sensing techniques. Journal of hydrology, **289**: 145-164. DOI: 10.1016/j.jhydrol.2003.11.038.

Monin A, Obukhov A. 1954. Basic laws of turbulent mixing in the surface layer of the atmosphere. Contrib. Geophys. Inst. Acad. Sci. USSR, **151**: 163-187.

Moran MS, Hymer DC, Qi J, Kerr Y. 2002. Comparison of ERS-2 SAR and Landsat TM imagery for monitoring agricultural crop and soil conditions. Remote Sens Environ, **79**: 243-252.

Moran MS, Inoue Y, Barnes EM. 1997. Opportunities and limitations for image-based remote sensing in precision crop management. Remote Sens Environ, **61**: 319-346. DOI: 10.1016/S0034-4257(97)00045-X.

Moran MS, Rahman AF, Washburne JC, Goodrich DC, Weltz MA, Kustas WP. 1996. Combining the Penman-Monteith equation with measurements of surface temperature and reflectance to estimate evaporation rates of semiarid grassland. Agric. For. Meteorol., **80**: 87-109. DOI: 10.1016/0168-1923(95)02292-9.

Morse A, Tasumi M, Allen RG, Kramber WJ. 2000. Application of the SEBAL methodology for estimating consumptive use of water and streamflow depletion in the Bear River Basin of Idaho through remote sensing. Idaho Department of Water Resources–University of Idaho.

Nash JE, Sutcliffe JV. 1970. River flow forecasting through conceptual models part I — A discussion of principles. Journal of hydrology, **10**: 282-290. DOI: 10.1016/0022-1694(70)90255-6.

Niemann JD, Lehman B, Gates T, Hallberg N, Elhaddad A. 2011. Impact of Shallow Groundwater on Evapotranspiration Losses from Uncultivated Land in an Irrigated River Valley. Journal of irrigation and drainage engineering, **137**: 501-512. DOI: doi:10.1061/(ASCE)IR.1943-4774.0000356.

Omernik JM. 1987. Map Supplement: Ecoregions of the Conterminous United States. Annals of the Association of American geographers, **77**: 118-125. DOI: 10.2307/2569206.

Owe M, Van De Griend AA. 1990. Daily surface moisture model for large area semiarid land application with limited climate data. Journal of hydrology, **121**: 119-132. DOI: 10.1016/0022-1694(90)90228-P.

Prueger JH, Kustas WP, Hipps LE, Hatfield JL. 2004. Aerodynamic parameters and sensible heat flux estimates for a semi-arid ecosystem. Journal of Arid Environments, **57**: 87-100. DOI: 10.1016/S0140-1963(03)00090-9.

Qi Y, Dennison PE, Spencer J, Riano D. 2012. Monitoring Live Fuel Moisture Using Soil Moisture and Remote Sensing Proxies. Fire Ecol, **8**: 71-87. DOI: 10.4996/fireecology.0803071.

Roerink GJ, Su Z, Menenti M. 2000. S-SEBI: A simple remote sensing algorithm to estimate the surface energy balance. Physics and Chemistry of the Earth, Part B: Hydrology, Oceans and Atmosphere, **25**: 147-157. DOI: 10.1016/S1464-1909(99)00128-8.

Santos CACd, Bezerra BG, Silva BBd, Rao TVR. 2010. Assessment of daily actual evapotranspiration with SEBAL and S-SEBI algorithms in cotton crop. Revista Brasileira de Meteorologia, **25**: 383-392.

Scott CA, Bastiaanssen WGM, Ahmad MUD. 2003. Mapping root zone soil moisture using remotely sensed optical imagery. J. Irrig. Drainage Eng-ASCE, **129**: 326-335. DOI: 10.1061/(Asce)0733-9437(2003)129:5(326).

Seelan SK, Laguette S, Casady GM, Seielstad GA. 2003. Remote sensing applications for precision agriculture: A learning community approach. Remote Sens Environ, **88**: 157-169.

Sellers PJ, Hall FG, Asrar G, Strebel D, Murphy R. 1992. An overview of the first international satellite land surface climatology project (ISLSCP) field experiment (FIFE). Journal of Geophysical Research: Atmospheres (1984–2012), **97**: 18345-18371.

Shuttleworth W, Gurney R, Hsu A, Ormsby J. 1989. FIFE: the variation in energy partition at surface flux sites. IAHS Publ, **186**: 67-74.

Smith EA, Hsu AY, Crosson WL, Field RT, Fritschen LJ, Gurney RJ, Kanemasu ET, Kustas WP, Nie D, Shuttleworth WJ, Stewart JB, Verma SB, Weaver HL, Wesely ML. 1992. Area-averaged surface fluxes and their time-space variability over the FIFE experimental domain. Journal of Geophysical Research: Atmospheres, **97**: 18599-18622. DOI: 10.1029/91jd03060.

Stevens MR, Dupree JA, Kuzmiak JM. 2008. Temporal and Spatial Variations in Precipitation, Streamflow, Suspended-sediment Loads and Yields, and Land-condition Trend Analysis at the US Army Piñon Canyon Maneuver Site, Las Animas County, Colorado, 1983 Through 2007. US Department of the Interior, US Geological Survey.

Stisen S, Sandholt I, Nørgaard A, Fensholt R, Jensen KH. 2008. Combining the triangle method with thermal inertia to estimate regional evapotranspiration — Applied to MSG-SEVIRI data in the Senegal River basin. Remote Sens Environ, **112**: 1242-1255. DOI: 10.1016/j.rse.2007.08.013.

Su Z. 1999. The Surface Energy Balance System (SEBS) for estimation of turbulent heat fluxes. Hydrology and Earth System Sciences, **6**: 85-100.

Thoma DP, Moran MS, Bryant R, Rahman MM, Collins CDH, Keefer TO, Noriega R, Osman I, Skrivin SM, Tischler MA, Bosch DD, Starks PJ, Peters-Lidard CD. 2008. Appropriate scale of soil moisture retrieval from high resolution radar imagery for bare and minimally vegetated soils. Remote Sens Environ, **112**: 403-414. DOI: 10.1016/j.rse.2007.06.021.

Topp GC, Davis JL, Annan AP. 1980. Electromagnetic determination of soil water content: Measurements in coaxial transmission lines. Water Resources Research, **16**: 574-582. DOI: 10.1029/WR016i003p00574.

Tripp DR, Niemann JD. 2008. Evaluating the parameter identifiability and structural validity of a probability-distributed model for soil moisture. Journal of hydrology, **353**: 93-108. DOI: 10.1016/j.jhydrol.2008.01.028.

Ulaby FT, Dubois PC, van Zyl J. 1996. Radar mapping of surface soil moisture. Journal of hydrology, **184**: 57-84. DOI: 10.1016/0022-1694(95)02968-0.

Verstraeten W, Veroustraete F, Feyen J. 2008. Assessment of Evapotranspiration and Soil Moisture Content Across Different Scales of Observation. Sensors, **8**: 70-117.

Von Guerard P, Abbott P, Nickless RC. 1987. Hydrology of the US Army Pinon Canyon Maneuver Site, Las Animas County, Colorado. United States Geological Survey.

Walker JP, Houser PR, Willgoose GR. 2004. Active microwave remote sensing for soil moisture measurement: a field evaluation using ERS-2. Hydrological processes, **18**: 1975-1997. DOI: 10.1002/hyp.1343.

Weaver JE. 1958. Summary and Interpretation of Underground Development in Natural Grassland Communities. Ecological Monographs, **28**: 55-78. DOI: 10.2307/1942275.

West NE, Moore R, Valentine K, Law L, Ogden P, Pinkney F, Tueller P, Robertson J, Beetle A. 1972. Galleta: Taxonomy, ecology and management of Hilaria jamesii on western rangelands. Utah Agricultural Experiment Station.

Western AW, Grayson RB, Blöschl G. 2002. Scaling of soil moisture: A hydrologic perspective. Annual Review of Earth and Planetary Sciences, **30**: 149-180. DOI: 10.1146/annurev.earth.30.091201.140434.

Yebra M, Dennison PE, Chuvieco E, Riaño D, Zylstra P, Hunt Jr ER, Danson FM, Qi Y, Jurdao S. 2013. A global review of remote sensing of live fuel moisture content for fire danger assessment: Moving towards operational products. Remote Sens Environ, **136**: 455-468. DOI: 10.1016/j.rse.2013.05.029.

LIST OF ABBREVIATIONS

ASCE	American Society of Civil Engineers	MRE	Mean relative error
ASTER	Advanced Spaceborne Thermal Emission and Reflection Radiometer	NDVI	Normalized difference vegetation index
AVHRR	Advanced Very High Resolution Radiometer	NEGU	Northeast Gully (CSU PCMS field)
BIGA	USGS Field, see Table 2	NLCD	National Land Cover Data
CANT	USGS Field, see Table 2	NRCS	Natural Resources Conservation Service
CoAgMet	Colorado Agricultural Meteorological Network	NSCE	Nash Sutcliffe Coefficient of Efficiency
CSI	Campbell Scientific	PCMS	Piñon Canyon Maneuver Site
CSU	Colorado State University	ReSET	Remote Sensing Evapotranspiration
CSU LARV	CSU Lower Arkansas River Valley	RMSE	Root mean square error
CSU PCMS	CSU Piñon Canyon Maneuver Site	*s*	Degree of saturation
DEM	Digital Elevation Model	SAR	Synthetic Aperture Radar
ECHIVAL	European International Project on Climatic and Hydrological Interactions between the Vegetation, the Atmosphere and the Land-surface	SEBAL	Surface Energy Balance Algorithm for Land
EFEDA	ECHIVAL Field Experiment in Desertification-Threatened Areas	SEBS	Surface Energy Balance System
EPA	Environmental Protection Agency	S-SEBI	Simplified Surface Energy Balance Index
ET	Evapotranspiration	SWGU	Southwest Gully (CSU PCMS field)
FIFE	First ISCLCP Field Experiment	TDR	Time domain reflectometry
ISCLCP	International Satellite Land Surface Climatology Project	UBEN	USGS Field, see Table 2
K_a	Apparent permittivity	UNGU	Ungullied (CSU PCMS field)
LAI	Leaf area index	USGS	United States Geological Survey
LARV	Lower Arkansas River Valley	USGS PCMS	USGS Piñon Canyon Maneuver Site
MAE	Mean absolute error	θ	Volumetric soil moisture
METRIC	Mapping Evapotranspiration at High Resolution with Internalized Calibration	Λ	Evaporative fraction
MODIS	Moderate-resolution Imaging Spectroradimeter		